

SLOT ANTENNA ON A CONDUCTING ELLIPTIC CYLINDER COATED BY NONCONFOCAL CHIRAL MEDIA

B. N. Khatir and A. R. Sebak

Department of Electrical and Computer Engineering
Concordia University
1455 de Maisonneuve Blvd. W., Montreal, Quebec, H3G 1M8, Canada

Abstract—The characteristics of a slot antenna on a perfectly conducting elliptic cylinder coated by nonconfocal chiral media are investigated. The structure is fed with a line source or plane wave. The analysis is carried out by expressing the fields in and around the cylinder in terms of Mathieu and modified Mathieu functions using the separation of variable and exact boundary value technique. The unknown aperture field is expressed in terms of Fourier series with unknown expansion coefficients. The expansion coefficients are found by applying the boundary conditions on different surfaces and employing the addition theorem and orthogonality properties of the Mathieu functions. For TM and TE cases some numerical results of the antenna gain for co- and cross-polarized waves are presented and discussed.

1. INTRODUCTION

Slot antennas are widely used in many practical applications such as radar and satellite communications, space vehicles, aircraft, missiles, and in standard desktop microwave devices for research purposes. The main advantages of slot antennas are adaptability, lightweight, design simplicity, ease of fabrication, high power capability, greater control of the radiation pattern compared to line antennas, and wider bandwidth compared to microstrip patch antennas. Silver and Saunders [1] have developed general expressions for the external field produced by a slot of arbitrary shape in the wall of an infinite circular cylinder. Wait [2] has published a comprehensive theoretical

Corresponding author: B. N. Khatir (b_najjar@ece.concordia.ca).

treatment of slots on cylindrical surfaces, i.e., circular and elliptical cylinders. Many kinds of slot antennas are theoretically analyzed by Wolff [3]. Extensive works is reported on investigating the characteristics of slotted antenna on circular cylinder coated by materials, i.e., dielectric [4, 5]. Other investigations are reported as well about slotted antennas on elliptic conducting cylinder. These include the radiation conductance [6], radiation patterns [7], and coupling properties of slotted elliptic cylinder [8], scattering by slotted elliptic cylinder [9], and characteristics of slotted elliptic cylinder coated by materials [10–14]. In most of the investigations on slotted cylinders, the aperture field is assumed as a known field. However, some work about non coated slotted elliptic cylinder [8] and dielectric/metamaterial coated slotted elliptic cylinder [14] with unknown aperture field are reported, as well.

A slotted cylinder coated by materials offers more control of the radiation power. Dielectric is one of the most used materials for this purpose. However, other kind of materials (i.e., isorefractive, metamaterial, and chiral media) with special electromagnetic wave propagation properties have recently become the subject of intensive studies [13–22]. Chiral media is a reciprocal medium characterized by different phase velocities for right and left handed circularly polarized waves. Chiral media responds with both electric and magnetic polarization to either electric or magnetic excitation. Chiral objects can generate both co- and cross-polarized fields simultaneously which is an advantage for some applications. They can be found in nature, or made artificially.

In this paper, characteristics of a slot antenna on a perfectly conducting elliptic cylinder coated by nonconfocal chiral media are investigated. The analysis is based on using the separation of variable and exact boundary value technique, and using the elliptic cylindrical coordinates system and Mathieu functions. The unknown aperture field is expressed in terms of Fourier series expansion with unknown coefficients. The formulation of the problem for TM case is introduced. The system of linear equations is solved using standard numerical techniques, to generate numerical results. Numerical results of the antenna gain for co- and cross-polarized waves are presented and discussed.

2. FORMULATIONS

Consider Cartesian coordinates system (x_c, y_c, z_c) or elliptic cylindrical coordinates system (ξ_c, η_c, z_c) as a local coordinates system, and (x, y, z) or (ξ, η, z) as a global coordinates system. A perfectly conducting

elliptic cylinder with semi-focal length f_c , semi-major axis a_c , and semi-minor axis b_c is centered at the origin of the local coordinates system. It has an axial slot along the z_c -axis with angular width $\eta_{c2} - \eta_{c1}$. This cylinder coated by a nonconfocal elliptic cylinder which is located at the origin of the global coordinates system with semi-focal length f , semi-major axis a , and semi-minor axis b . The major axis (x_c -axis) of the local coordinates system with respect to the major axis (x -axis) of the global coordinates system is oriented by an angle α , and its center with respect to center of the global coordinates system is given by the polar coordinates system (d, β) . A cross section of this geometry in the x - y plane is shown in Figure 1 which includes three regions.

In general, the inner region of the conducting cylinder (region 1), can be free space, dielectric, or metamaterial. The coated region (region 2), can be free space, dielectric, isorefractive, metamaterial, or chiral media. The region 3 is free space. Considering a transverse magnetic (TM) polarized wave incident, the eigenfunction expansions in regions 1 and 2 can be expressed in terms of local coordinates system, while in region 3 they can be expressed in terms of global coordinates system.

In the transmit mode, assume a line source is located in region 1, and in the receiving or coupling mode, a plane wave is incident from region 3. The incident electric field, for an electric line source of unit amplitude which is located at (ξ_0, η_0) in region 1 is given by [8]

$$E_{z_c}^i = \sum_m A_{\epsilon_m} R_{\epsilon_m}^{(4)}(c_1, \xi_c) S_{\epsilon_m}(c_1, \eta_c), \quad \xi_c \geq \xi_0 \quad (1)$$

$$A_{\epsilon_n} = 4R_{\epsilon_n}^{(1)}(c_1, \xi_0) S_{\epsilon_n}(c_1, \eta_0) / N_{\epsilon_n}(c_1) \quad (2)$$

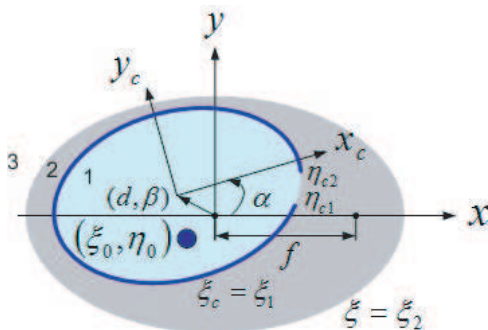


Figure 1. Geometry of slotted elliptic cylinder.

and for a plane wave is given by

$$E_z^i = \sum_m A_{\epsilon m} R_{\epsilon m}^{(1)}(c_3, \xi) S_{\epsilon m}(c_3, \eta) \quad (3)$$

$$A_{\epsilon n} = j^n \sqrt{8\pi} E_0 S_{\epsilon n}(c_3, \cos \phi^i) / N_{\epsilon n}(c_3) \quad (4)$$

where S is the angular Mathieu function, $R^{(l)}$ is the l th kind of radial Mathieu function ($l = 1, \dots, 4$), $c_1 = k_1 f_c$, $c_3 = k_3 f$, k_l is wave number in region l , subscripts e and o denote even and odd types, respectively. Also summation (Σ) starts from 0 for even type and from 1 for odd type functions, E_0 is the amplitude of the incident field, ϕ^i is the incident angle with respect to the major axis of the corresponding (local or global) coordinates system, and

$$N_{\epsilon n}(c_l) = \int_0^{2\pi} [S_{\epsilon n}(c_l, \eta^+)]^2 d\eta^+, \quad (5)$$

$$\xi_0 = \cosh^{-1} \left\{ \left[\frac{1}{2} \left(\frac{\rho_0^2}{f_0^2} + 1 \right) + \sqrt{\frac{1}{4} \left(\frac{\rho_0^2}{f_0^2} + 1 \right)^2 - \frac{x_0^2}{f_0^2}} \right]^{1/2} \right\} \quad (6)$$

$$\eta_0 = \cos^{-1} \left(\frac{x_0}{f_0 \cosh \xi_0} \right) \quad (7)$$

$$x_0 = \rho_0 \cos \phi^i \quad (8)$$

$\eta^+ = \eta_c$ (or η) if $l = 1$ (or 3), $f_0 = f_c$ (or f) if source located in region 1 (or 3), and ρ_0 is the radial distance from the origin of the circular cylindrical coordinates system to the source location. The origin of the circular cylinder is center of the local coordinates system if source located in region 1, and it is center of the global coordinates system if source located in region 3.

The corresponding incident magnetic fields in the η_c and η directions (for regions 1 and 3) can be obtained by Maxwell's equations. For example for region 1,

$$H_{\eta_c}^i = \frac{-j}{\omega \mu_1 h_c} \frac{\partial E_{z_c}^i}{\partial \xi_c} \quad (9)$$

where μ_1 is permeability of region 1 and h_c is a scale factor in elliptic cylindrical coordinates systems,

$$h_c = f_c \sqrt{\cosh^2 \xi_c - \cos^2 \eta_c}. \quad (10)$$

The problem formulation for chiral medium is more complicated and general compared to achiral medium. The constitutive relationships for a chiral medium are given by [19]

$$\vec{D} = \epsilon_c \vec{E} - j\gamma\mu\vec{H} \quad (11)$$

$$\vec{B} = \mu\vec{H} + j\gamma\mu\vec{E} \quad (12)$$

$$\epsilon_c = \epsilon + \mu\gamma^2 \quad (13)$$

where \vec{D} , \vec{B} , and \vec{H} are the electric flux density, magnetic flux density, and magnetic field, respectively. Also ϵ_c is the effective permittivity of the chiral medium, ϵ is the permittivity, μ is the permeability, and γ is the chiral admittance of the medium. If μ , ϵ , or γ is complex the media is lossy. If $\gamma = 0$, then (11) and (12) reduce to an achiral medium. The chiral wave numbers are given by [19]

$$k_R = \omega\sqrt{\mu\epsilon_c} + \omega\mu\gamma \quad (14)$$

$$k_L = \omega\sqrt{\mu\epsilon_c} - \omega\mu\gamma \quad (15)$$

where k_R and k_L , are the propagation constants of right and left circularly polarized waves, respectively.

In presence of chiral media, the fields may be expanded as an infinite sum of vector wave functions, \vec{M}_m and \vec{N}_m [19], which are related by

$$\nabla \times \vec{N}_m = k\vec{M}_m \quad (16)$$

$$\nabla \times \vec{M}_m = k\vec{N}_m. \quad (17)$$

In elliptic cylindrical coordinates system (ξ, η, z) , \vec{M}_m and \vec{N}_m can be written as

$$\vec{N}_m^{(l)}(k) = \hat{u}_z R_{\epsilon_m}^{(l)}(c, \xi) S_{\epsilon_m}(c, \eta) \quad (18)$$

$$\begin{aligned} \vec{M}_m^{(l)}(k) &= \frac{1}{k} \nabla \times \vec{N}_m^{(l)}(k) = \hat{u}_\xi M_\xi + \hat{u}_\eta M_\eta \\ &= \hat{u}_\xi \frac{1}{kh} R_{\epsilon_m}^{(l)}(c, \xi) S'_{\epsilon_m}(c, \eta) - \hat{u}_\eta \frac{1}{kh} R_{\epsilon_m}^{(l)'}(c, \xi) S_{\epsilon_m}(c, \eta) \end{aligned} \quad (19)$$

where prim indicates the derivative with respect to the arguments, ξ for R , and η for S functions.

Therefore, the fields in region 1 will have TM_Z and TE_Z components, and the electric field is expanded as

$$\vec{E}^1 = \sum_m \left[B1_{\epsilon_m} \vec{M}_m^{(1)}(k_1) + B2_{\epsilon_m} \vec{N}_m^{(1)}(k_1) \right] \quad (20)$$

where $B1_{\epsilon_m}$ and $B2_{\epsilon_m}$ are unknown expansion coefficients. The corresponding magnetic field can be written as

$$\vec{H}^1 = \frac{j}{\sqrt{\mu_1/\epsilon_1}} \sum_m \left[B1_{\epsilon_m} \vec{N}_m^{(1)}(k_1) + B2_{\epsilon_m} \vec{M}_m^{(1)}(k_1) \right]. \quad (21)$$

The unknown aperture fields on the slot are expressed in terms of sinusoidal Fourier representation of even and odd parts, i.e.,

$$E_{\eta_c}^a(\eta_c) = \frac{-1}{k_1 h_c} \sum_m b1_{\epsilon_m} C S_{\epsilon_m}(\eta_c) \quad (22)$$

$$E_{z_c}^a(\eta_c) = \sum_m b2_{\epsilon_m} C S_{\epsilon_m}(\eta_c) \quad (23)$$

$$C S_{\epsilon_m}(\eta_c) = \begin{cases} \cos \frac{2m\pi}{\eta_{c2} - \eta_{c1}} \eta_c \\ \sin \frac{2m\pi}{\eta_{c2} - \eta_{c1}} \eta_c \end{cases} \quad (24)$$

where $b1_{\epsilon_m}$ and $b2_{\epsilon_m}$ are unknown expansion coefficients.

In region 2, the eigenfunction expansion must account for the polarization rotation inherent to chiral media. In a z -independent problem, these result in a coupling between the TM_Z and TE_Z fields, which prevents the eigenfunction expansion from being written as a simple superposition of TM_Z and TE_Z fields. However, the eigenfunction expansion can be written as a superposition of right and left hand circularly polarized fields. This is done by combining the vector wave functions \vec{M}_m and \vec{N}_m , to form right and left circularly polarized vector wave functions

$$\vec{E}_{Rm}^{(l)} = \vec{M}_m^{(l)}(k_R) + \vec{N}_m^{(l)}(k_R) \quad (25)$$

$$\vec{E}_{Lm}^{(l)} = -\vec{M}_m^{(l)}(k_L) + \vec{N}_m^{(l)}(k_L). \quad (26)$$

The electric field in the chiral medium may be then represented as

$$\begin{aligned} \vec{E}^2 &= \vec{E}_R^2 + \vec{E}_L^2 \\ &= \sum_m C1_{\epsilon_m} \left[\vec{M}_m^{(1)}(k_R) + \vec{N}_m^{(1)}(k_R) \right] + \sum_m C2_{\epsilon_m} \left[-\vec{M}_m^{(1)}(k_L) + \vec{N}_m^{(1)}(k_L) \right] \\ &+ \sum_m D1_{\epsilon_m} \left[\vec{M}_m^{(2)}(k_R) + \vec{N}_m^{(2)}(k_R) \right] + \sum_m D2_{\epsilon_m} \left[-\vec{M}_m^{(2)}(k_L) + \vec{N}_m^{(2)}(k_L) \right] \\ &= \hat{u}_{\xi_c} \frac{1}{h_c} \left\{ \frac{1}{k_R} \sum_m C1_{\epsilon_m} R_{\epsilon_m}^{(1)}(c_R, \xi_c) S'_{\epsilon_m}(c_R, \eta_c) \right. \end{aligned}$$

$$\begin{aligned}
 & -\frac{1}{k_L} \sum_m C2_{\circ m} R_{\circ m}^{(1)}(c_L, \xi_c) S'_{\circ m}(c_L, \eta_c) \\
 & +\frac{1}{k_R} \sum_m D1_{\circ m} R_{\circ m}^{(2)}(c_R, \xi_c) S'_{\circ m}(c_R, \eta_c) \\
 & \left. -\frac{1}{k_L} \sum_m D2_{\circ m} R_{\circ m}^{(2)}(c_L, \xi_c) S'_{\circ m}(c_L, \eta_c) \right\} \\
 & -\hat{u}_{\eta_c} \frac{1}{\hbar c} \left\{ \frac{1}{k_R} \sum_m C1_{\circ m} R_{\circ m}^{(1)'}(c_R, \xi_c) S_{\circ m}(c_R, \eta_c) \right. \\
 & -\frac{1}{k_L} \sum_m C2_{\circ m} R_{\circ m}^{(1)'}(c_L, \xi_c) S_{\circ m}(c_L, \eta_c) \\
 & +\frac{1}{k_R} \sum_m D1_{\circ m} R_{\circ m}^{(2)'}(c_R, \xi_c) S_{\circ m}(c_R, \eta_c) \\
 & \left. -\frac{1}{k_L} \sum_m D2_{\circ m} R_{\circ m}^{(2)'}(c_L, \xi_c) S_{\circ m}(c_L, \eta_c) \right\} \\
 & +\hat{u}_{z_c} \left\{ \sum_m C1_{\circ m} R_{\circ m}^{(1)}(c_R, \xi_c) S_{\circ m}(c_R, \eta_c) \right. \\
 & +\sum_m C2_{\circ m} R_{\circ m}^{(1)}(c_L, \xi_c) S_{\circ m}(c_L, \eta_c) \\
 & +\sum_m D1_{\circ m} R_{\circ m}^{(2)}(c_R, \xi_c) S_{\circ m}(c_R, \eta_c) \\
 & \left. +\sum_m D2_{\circ m} R_{\circ m}^{(2)}(c_L, \xi_c) S_{\circ m}(c_L, \eta_c) \right\} \tag{27}
 \end{aligned}$$

where $c_R = k_R f c$, $c_L = k_L f c$, $C1_{\circ m}$, $C2_{\circ m}$, $D1_{\circ m}$, and $D2_{\circ m}$ are unknown expansion coefficients. The corresponding magnetic field can be written as

$$\begin{aligned}
 \vec{H}^2 &= \frac{j}{\sqrt{\mu_2/\epsilon_2}} \left\{ \vec{E}_R^2 - \vec{E}_L^2 \right\} \\
 &= \frac{j}{\sqrt{\mu_2/\epsilon_2}} \left\{ \sum_m C1_{\circ m} \left[\vec{M}_m^{(1)}(k_R) + \vec{N}_m^{(1)}(k_R) \right] \right. \\
 & \quad \left. + \sum_m C2_{\circ m} \left[\vec{M}_m^{(1)}(k_L) - \vec{N}_m^{(1)}(k_L) \right] \right\}
 \end{aligned}$$

$$\begin{aligned}
& + \sum_m D1_{\epsilon m} \left[\vec{M}_m^{(2)}(k_R) + \vec{N}_m^{(2)}(k_R) \right] \\
& + \sum_m D2_{\epsilon m} \left[\vec{M}_m^{(2)}(k_L) - \vec{N}_m^{(2)}(k_L) \right] \Big\} \quad (28)
\end{aligned}$$

The fields in region 3 will have TM_Z and TE_Z components. Therefore, the electric field is expanded as

$$\vec{E}^3 = \sum_m \left[F1_{\epsilon m} \vec{M}_m^{(4)}(k_3) + F2_{\epsilon m} \vec{N}_m^{(4)}(k_3) \right] \quad (29)$$

where $F1_{\epsilon m}$ and $F2_{\epsilon m}$ are unknown expansion coefficients. The corresponding magnetic field can be written as

$$\vec{H}^3 = \frac{j}{\sqrt{\mu_3/\epsilon_3}} \sum_m \left[F1_{\epsilon m} \vec{N}_m^{(4)}(k_3) + F2_{\epsilon m} \vec{M}_m^{(4)}(k_3) \right]. \quad (30)$$

The unknown expansion coefficients, $B1_{\epsilon m}$, $B2_{\epsilon m}$, $b1_{\epsilon m}$, $b2_{\epsilon m}$, $C1_{\epsilon m}$, $C2_{\epsilon m}$, $D1_{\epsilon m}$, $D2_{\epsilon m}$, $F1_{\epsilon m}$, and $F2_{\epsilon m}$ may be determined by imposing the boundary conditions on the surfaces of slotted and coated cylinders defined by $\xi_c = \xi_1$ and $\xi = \xi_2$. The boundary conditions at $\xi = \xi_2$ can be applied after the transformation of the field components inside the coating (region 2) in terms of the global coordinates system. This can be done using the addition theorem of Mathieu functions [23], so that components $E_{\eta_c}^2$, $E_{z_c}^2$, $H_{\eta_c}^2$, and $H_{z_c}^2$ in the local coordinates system change to similar components (E_{η}^2 , E_z^2 , H_{η}^2 , and H_z^2 , respectively) in the global coordinates system, as

$$\begin{aligned}
E_{\eta}^2 = & \frac{-1}{h} \left\{ \frac{1}{k_R} \sum_m C1_{\epsilon m} \sum_l \left[W E_{\epsilon l m} R_{el}^{(1)'}(c_{R2}, \xi) S_{el}(c_{R2}, \eta) \right. \right. \\
& + W O_{\epsilon l m} R_{ol}^{(1)'}(c_{R2}, \xi) S_{ol}(c_{R2}, \eta) \Big] \\
& - \frac{1}{k_L} \sum_m C2_{\epsilon m} \sum_l \left[W E_{\epsilon l m} R_{el}^{(1)'}(c_{L2}, \xi) S_{el}(c_{L2}, \eta) \right. \\
& + W O_{\epsilon l m} R_{ol}^{(1)'}(c_{L2}, \xi) S_{ol}(c_{L2}, \eta) \Big] \\
& + \frac{1}{k_R} \sum_m D1_{\epsilon m} \sum_l \left[W E_{\epsilon l m} R_{el}^{(2)'}(c_{R2}, \xi) S_{el}(c_{R2}, \eta) \right. \\
& + W O_{\epsilon l m} R_{ol}^{(2)'}(c_{R2}, \xi) S_{ol}(c_{R2}, \eta) \Big]
\end{aligned}$$

$$\begin{aligned}
 & -\frac{1}{k_L} \sum_m D2_{\epsilon m} \sum_l \left[W E_{\epsilon l m} R_{el}^{(2)'}(c_{L2}, \xi) S_{el}(c_{L2}, \eta) \right. \\
 & \left. + W O_{\epsilon l m} R_{ol}^{(2)'}(c_{L2}, \xi) S_{ol}(c_{L2}, \eta) \right] \} \quad (31)
 \end{aligned}$$

$$\begin{aligned}
 E_z^2 = & \sum_m C1_{\epsilon m} \sum_l \left[W E_{\epsilon l m} R_{el}^{(1)}(c_{R2}, \xi) S_{el}(c_{R2}, \eta) \right. \\
 & \left. + W O_{\epsilon l m} R_{ol}^{(1)}(c_{R2}, \xi) S_{ol}(c_{R2}, \eta) \right] \\
 & + \sum_m C2_{\epsilon m} \sum_l \left[W E_{\epsilon l m} R_{el}^{(1)}(c_{L2}, \xi) S_{el}(c_{L2}, \eta) \right. \\
 & \left. + W O_{\epsilon l m} R_{ol}^{(1)}(c_{L2}, \xi) S_{ol}(c_{L2}, \eta) \right] \\
 & + \sum_m D1_{\epsilon m} \sum_l \left[W E_{\epsilon l m} R_{el}^{(2)}(c_{R2}, \xi) S_{el}(c_{R2}, \eta) \right. \\
 & \left. + W O_{\epsilon l m} R_{ol}^{(2)}(c_{R2}, \xi) S_{ol}(c_{R2}, \eta) \right] \\
 & + \sum_m D2_{\epsilon m} \sum_l \left[W E_{\epsilon l m} R_{el}^{(2)}(c_{L2}, \xi) S_{el}(c_{L2}, \eta) \right. \\
 & \left. + W O_{\epsilon l m} R_{ol}^{(2)}(c_{L2}, \xi) S_{ol}(c_{L2}, \eta) \right] \quad (32)
 \end{aligned}$$

$$\begin{aligned}
 H_\eta^2 = & \frac{-j}{h\sqrt{\mu_2/\epsilon_2}} \left\{ \frac{1}{k_R} \sum_m C1_{\epsilon m} \sum_l \left[W E_{\epsilon l m} R_{el}^{(1)'}(c_{R2}, \xi) S_{el}(c_{R2}, \eta) \right. \right. \\
 & \left. \left. + W O_{\epsilon l m} R_{ol}^{(1)'}(c_{R2}, \xi) S_{ol}(c_{R2}, \eta) \right] \right. \\
 & + \frac{1}{k_L} \sum_m C2_{\epsilon m} \sum_l \left[W E_{\epsilon l m} R_{el}^{(1)'}(c_{L2}, \xi) S_{el}(c_{L2}, \eta) \right. \\
 & \left. + W O_{\epsilon l m} R_{ol}^{(1)'}(c_{L2}, \xi) S_{ol}(c_{L2}, \eta) \right] \\
 & + \frac{1}{k_R} \sum_m D1_{\epsilon m} \sum_l \left[W E_{\epsilon l m} R_{el}^{(2)'}(c_{R2}, \xi) S_{el}(c_{R2}, \eta) \right. \\
 & \left. + W O_{\epsilon l m} R_{ol}^{(2)'}(c_{R2}, \xi) S_{ol}(c_{R2}, \eta) \right] \\
 & \left. + \frac{1}{k_L} \sum_m D2_{\epsilon m} \sum_l \left[W E_{\epsilon l m} R_{el}^{(2)'}(c_{L2}, \xi) S_{el}(c_{L2}, \eta) \right. \right. \\
 & \left. \left. + W O_{\epsilon l m} R_{ol}^{(2)'}(c_{L2}, \xi) S_{ol}(c_{L2}, \eta) \right] \right\} \quad (33)
 \end{aligned}$$

$$\begin{aligned}
H_z^2 = & \frac{j}{\sqrt{\mu_2/\varepsilon_2}} \left\{ \sum_m C1_{\varepsilon m} \sum_l \left[WE_{\varepsilon l m} R_{el}^{(1)}(c_{R2}, \xi) S_{el}(c_{R2}, \eta) \right. \right. \\
& \left. \left. + WO_{\varepsilon l m} R_{ol}^{(1)}(c_{R2}, \xi) S_{ol}(c_{R2}, \eta) \right] \right. \\
& - \sum_m C2_{\varepsilon m} \sum_l \left[WE_{\varepsilon l m} R_{el}^{(1)}(c_{L2}, \xi) S_{el}(c_{L2}, \eta) \right. \\
& \left. \left. + WO_{\varepsilon l m} R_{ol}^{(1)}(c_{L2}, \xi) S_{ol}(c_{L2}, \eta) \right] \right. \\
& + \sum_m D1_{\varepsilon m} \sum_l \left[WE_{\varepsilon l m} R_{el}^{(2)}(c_{R2}, \xi) S_{el}(c_{R2}, \eta) \right. \\
& \left. \left. + WO_{\varepsilon l m} R_{ol}^{(2)}(c_{R2}, \xi) S_{ol}(c_{R2}, \eta) \right] \right. \\
& - \sum_m D2_{\varepsilon m} \sum_l \left[WE_{\varepsilon l m} R_{el}^{(2)}(c_{L2}, \xi) S_{el}(c_{L2}, \eta) \right. \\
& \left. \left. + WO_{\varepsilon l m} R_{ol}^{(2)}(c_{L2}, \xi) S_{ol}(c_{L2}, \eta) \right] \right\} \quad (34)
\end{aligned}$$

where $c_{R2} = k_{Rf}$, $c_{L2} = k_{Lf}$, and the l -summation (Σ) starts from 0 for even type (WE) and from 1 for odd type (WO). Details of WE and WO are given in [23].

Therefore, considering an electric line source in region 1, the boundary conditions at $\xi_c = \xi_1$ are

$$E_{\eta_c}^1 = \begin{cases} E_{\eta_c}^a, & \eta_{c1} < \eta_c < \eta_{c2} \\ 0, & \text{else} \end{cases} \quad (35)$$

$$E_{z_c}^i + E_{z_c}^1 = \begin{cases} E_{z_c}^a, & \eta_{c1} < \eta_c < \eta_{c2} \\ 0, & \text{else} \end{cases} \quad (36)$$

$$E_{\eta_c}^2 = \begin{cases} E_{\eta_c}^a, & \eta_{c1} < \eta_c < \eta_{c2} \\ 0, & \text{else} \end{cases} \quad (37)$$

$$E_{z_c}^2 = \begin{cases} E_{z_c}^a, & \eta_{c1} < \eta_c < \eta_{c2} \\ 0, & \text{else} \end{cases} \quad (38)$$

$$H_{\eta_c}^i + H_{\eta_c}^1 = H_{\eta_c}^2, \quad \eta_{c1} < \eta_c < \eta_{c2} \quad (39)$$

$$H_{z_c}^1 = H_{z_c}^2, \quad \eta_{c1} < \eta_c < \eta_{c2} \quad (40)$$

and the boundary conditions at $\xi = \xi_2$ are

$$E_{\eta}^2 = E_{\eta}^3 \quad (41)$$

$$E_z^2 = E_z^3 \quad (42)$$

$$H_{\eta}^2 = H_{\eta}^3 \quad (43)$$

$$H_z^2 = H_z^3. \tag{44}$$

For a plane wave excitation, the incident fields $E_{z_c}^i$ and $H_{\eta_c}^i$ should be removed from (36) and (39), and E_z^i and H_η^i added to right side of (42) and (43), respectively.

To find the unknown expansion coefficients, we substitute the corresponding expressions from (1)–(34) into (35)–(44). Multiplying both sides of obtained equations by appropriate angular functions, integrating over the counters, and using the orthogonality properties of Mathieu functions, the terms involving even functions decouple completely from those of odd functions, and vice versa. Finally, the unknown expansion coefficients can be found from the obtained equations system.

Once the unknown expansion coefficients are found, the antenna gain can be calculated. Due to the chiral medium, there are two (co- and cross-) polarization waves everywhere. The far zone co-polarized electric field is

$$E_z^3(\rho, \phi) = \sqrt{\frac{j}{k_3\rho}} e^{-jk_3\rho} \sum_m j^m F 2_{\sigma m} S_{\sigma m}(c_3, \cos \phi) \tag{45}$$

where ρ and ϕ denote the polar coordinates in the circular cylindrical coordinates system. The far zone cross-polarized electric field can be written as

$$E_\eta^3(\rho, \phi) = -\sqrt{\frac{j}{k_3\rho}} e^{-jk_3\rho} \sum_m j^{m+1} F 1_{\sigma m} S_{\sigma m}(c_3, \cos \phi). \tag{46}$$

The time-average power density in the far zone co-polarized field is

$$S(\rho, \phi) = \frac{1}{\sqrt{\mu_3/\varepsilon_3 k_3\rho}} \left| \sum_m j^m F 2_{\sigma m} S_{\sigma m}(c_3, \cos \phi) \right|^2. \tag{47}$$

The average power density of $S(\rho, \phi)$ over an imaginary cylindrical surface with radius ρ can be written

$$\begin{aligned} S_{av}(\rho) &= \frac{1}{2\pi} \int_0^{2\pi} S(\rho, \phi) d\phi \\ &= \frac{1}{2\pi \sqrt{\mu_3/\varepsilon_3 k_3\rho}} \sum_m |F 2_{\sigma m}|^2 N_{\sigma m}(c_3). \end{aligned} \tag{48}$$

Using (46), the corresponding power equations for cross-polarized field, similar to (47) and (48) can be found. The antenna gain is given by

$$G(\phi) = S(\rho, \phi)/S_{av}(\rho). \tag{49}$$

3. NUMERICAL RESULTS

Although the formulation is presented for the TM case, numerical results are given for both TM and TE cases. The selected numerical results are presented for a variety of geometrical and material parameters. In each case, the infinite series is terminated to include only N terms of both the even and odd functions, where N , in general, is a suitable truncation number proportional to the structure's electrical size and shape. After several simulations of different material and geometrical parameters, it is found that $N = 2k_R a + 3$ provides a very good solution accuracy for far zone fields. The infinite series of aperture fields is terminated to include only M terms of both the even and odd functions, where M , is a suitable truncation number proportional to the structure's electrical size and aperture width.

There are many ways to validate the formulation and associated software program. As the first example, consider a cylinder with very small cross section and whole slot ($\eta_{c2} - \eta_{c1} = 360^\circ$) coated by a chiral media. The scattered field from this cylinder should be the same as the scattered field from a pure chiral cylinder. Figure 2 shows the co- and cross-polarized scattering echo widths for a cylinder with a small cross section coated with nonconfocal chiral media. Inside the slotted cylinder is a dielectric with the same permeability and permittivity of the coated chiral media. The source is a TM polarized plane wave with incident angle $\phi^i = 180^\circ$. Other parameters are given on the figure. These results are in excellent agreement with the results given in [18, 20] for scattering echo widths due to a circular chiral cylinder.

Many other checks were also done by considering the fact that

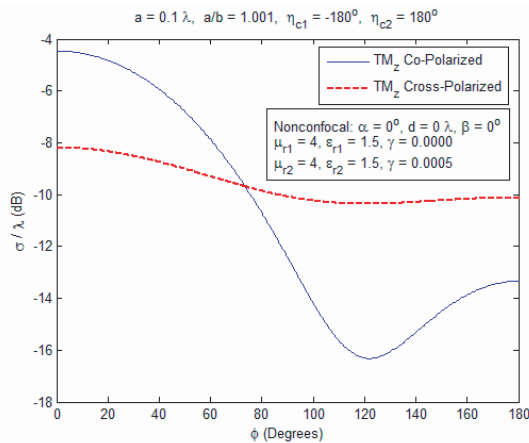


Figure 2. Scattering echo width from a circular chiral cylinder.

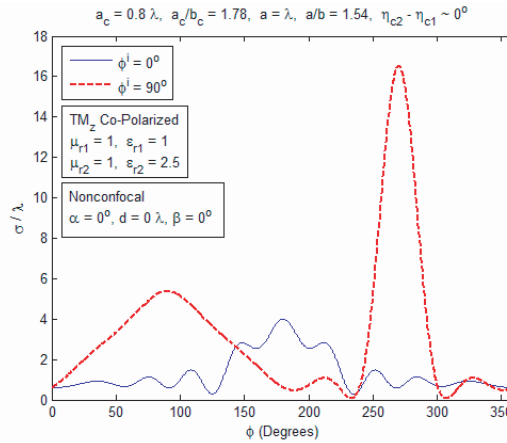


Figure 3. Scattering echo width from a narrow slotted elliptic cylinder coated by a nonconfocal dielectric.

the scattered field from a conducting elliptic cylinder with very narrow slot ($\eta_{c2} - \eta_{c1} \approx 0^\circ$) should be the same as the scattered field from a conducting elliptic cylinder without slot. In all considered cases with different geometrical and material parameters for TM and TE polarized waves, the calculated scattered fields from a narrow slotted cylinder coated by a confocal dielectric were completely agreement with the results given in [24] for a conducting cylinder coated by a confocal dielectric. Furthermore, as a second verification example, Figure 3 shows the scattering echo widths for a conducting elliptic cylinder coated by a nonconfocal dielectric when the slot angle width is very narrow. The source is a TM polarized plane wave with incident angles $\phi^i = 0^\circ$ and 90° . Inside the conducting cylinder is free space and other parameters are given on the figure. These results are very good agreement with the results given in [25] for scattering echo widths of conducting elliptic cylinder coated by a nonconfocal dielectric.

For the following examples, the effects of different geometries and material parameters on antenna gain are presented and discussed. More details of geometrical and material parameters are given on the figures.

Figures 4 and 5 show the effect of chirality on slot antenna gain. For both figures the nonconfocal coating cylinder is a chiral media with different chirality. An electric line source is located in the center of core cylinders and the excited wave is a TM polarized wave. Figure 4 shows the co-polarized antenna gain from the slotted elliptic cylinder with semi-major axis $a_c = \lambda$, axial ratio $a_c/b_c = 2$, and slot angle width 10°

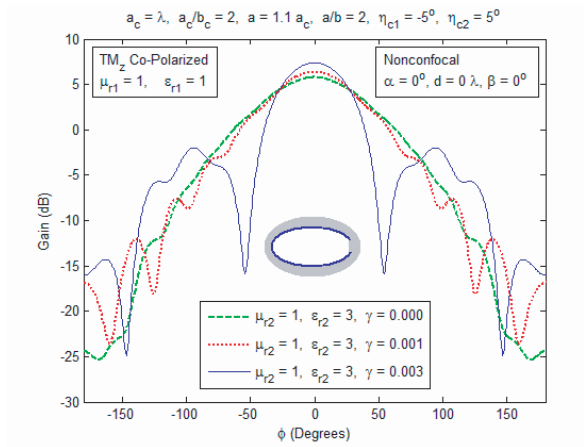


Figure 4. Effect of chirality on antenna gain in TM_z co-polarized.

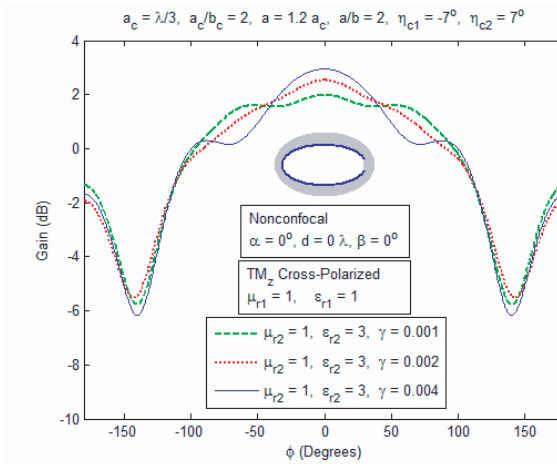


Figure 5. Effect of chirality on antenna gain in TM_z cross-polarized.

($\eta_{c1} = -5^\circ$ and $\eta_{c2} = 5^\circ$), coated by a cylinder with semi-major axis $a = 1.1a_c$ and axial ratio $a/b = 2$. Figure 5 shows the cross-polarized antenna gain from the slotted elliptic cylinder with semi-major axis $a_c = \lambda/3$, axial ratio $a_c/b_c = 2$, and slot angle width 14° ($\eta_{c1} = -7^\circ$ and $\eta_{c2} = 7^\circ$), coated by a cylinder with semi-major axis $a = 1.2a_c$ and axial ratio $a/b = 2$. As shown in these figures antenna gains increase (around 0°) by increasing of chirality.

One of the advantages of nonconfocal coating is, more material can be placed in front of slot. Figures 6 and 7 show the results for

the geometries in which the coating thicknesses in front of slots are more than the coating thicknesses of the other parts of conducting cylinders. The coated cylinders are nonconfocal chiral media with different chirality. Figure 6 shows the results for slotted elliptic cylinder with semi-major axis $a_c = \lambda/2$, axial ratio $a_c/b_c = 2$, and slot angle width 10° ($\eta_{c1} = 85^\circ$ and $\eta_{c2} = 95^\circ$) coated by a nonconfocal cylinder with semi-major axis $a = 0.75\lambda$ and axial ratio $a/b = 1.5$. A magnetic line source is located inside the elliptic core cylinder at $\rho_0 = \lambda/8$ and $\phi^i = \pi/2$, and the excited wave is a TE polarized wave. Figure 7 shows the results for slotted elliptic cylinder with semi-major axis $a_c = \lambda/3$, axial ratio $a_c/b_c = 2$, and slot angle width 10° ($\eta_{c1} = -5^\circ$ and $\eta_{c2} = 5^\circ$) coated by nonconfocal cylinder with semi-major axis $a = \lambda/2$, and axial ratio $a/b = 2$. An electric line source is located in the center of core cylinder and the excited wave is a TM polarized wave. As shown in Figures 6 and 7 the antenna gains at desired angles (90° and 0° , respectively) increase by increasing the chirality.

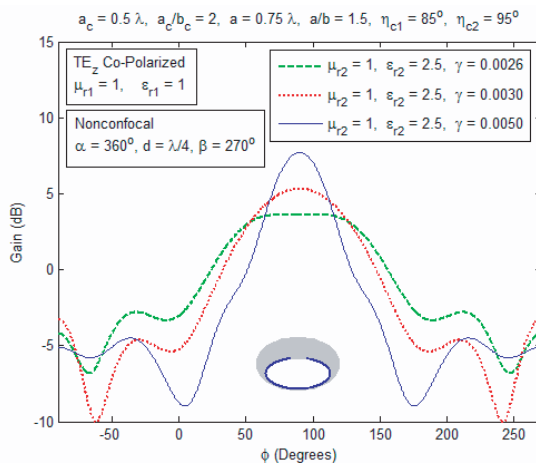


Figure 6. Effect of chirality on antenna gain in TE_z co-polarized.

Figure 8 shows the effect of coating thickness on co-polarized antenna gain for chiral media-coating with different chirality. In this geometry the slotted elliptic cylinder has semi-major axis $a_c = \lambda/3$, axial ratio $a_c/b_c = 3$, and slot angle width 10° ($\eta_{c1} = 85^\circ$ and $\eta_{c2} = 95^\circ$). A magnetic line source is located inside the elliptic core cylinder at $\rho_0 = \lambda/18$ and $\phi^i = \pi/2$, and the excited wave is a TE polarized wave. The coating axial ratio $a/b = 3$ and coating thicknesses are calculated from the semi-minor axis b_c . As shown in this figure, the antenna gain increases by increasing the chirality. Also for this

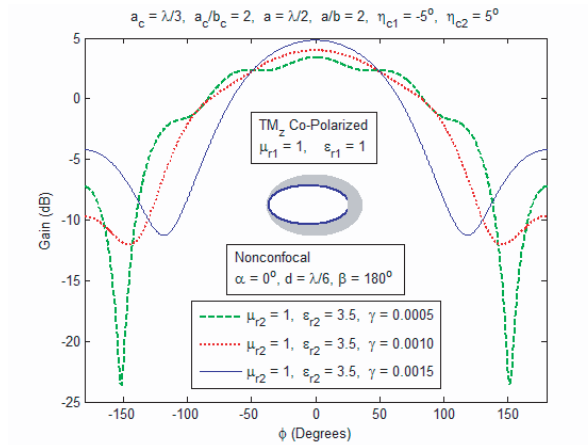


Figure 7. Effect of chirality on antenna gain in TM_z co-polarized.

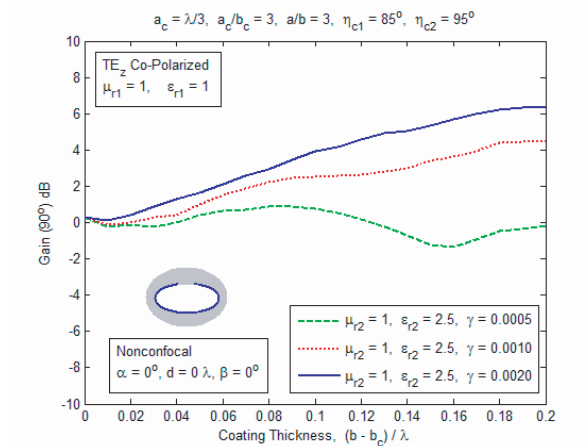


Figure 8. Effect of coating thickness and chirality on antenna gain in TE_z co-polarized.

geometry, antenna gain increases by increasing the coating thickness for chiral admittances $\gamma = 0.0010$ and $\gamma = 0.0020$.

Finally, the effects of coating thicknesses on antenna gain for coated materials dielectric, isorefractive, and chiral media are shown in Figures 9. In this geometry the slotted elliptical cylinder has semi-major axis $a_c = \lambda/3$, axial ratio $a_c/b_c = 3$, and slot angle width 20° ($\eta_{c1} = -10^\circ$ and $\eta_{c2} = 10^\circ$). An electric line source is located in the center of core cylinder, and the excited wave is a TM polarized wave. The coating axial ratio $a/b = 3$ and coating thicknesses are calculated

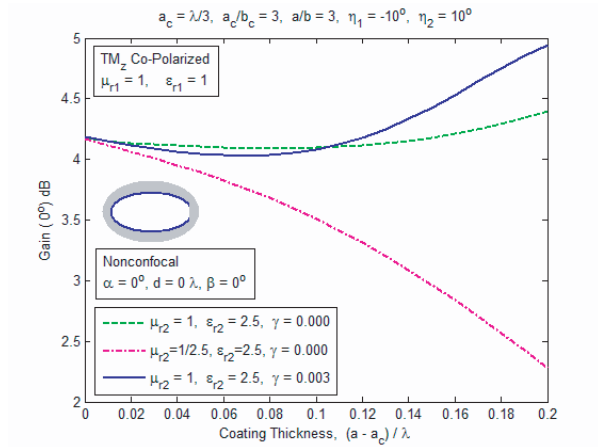


Figure 9. Effect of coating thickness on antenna gain in TM_z co-polarized.

from the semi-major axis a_c . As shown in this figure, by increasing the coating thickness, the gain due to isorefractive-coating decreases while the gains due to dielectric- and chiral media-coating increase for coating thickness more than 0.1λ .

4. CONCLUSION

A general solution to the problem of a slot antenna on a perfectly conducting elliptic cylinder coated by a nonconfocal chiral media is presented. The analysis is carried out by expressing the fields in and around the cylinder in terms of Mathieu and modified Mathieu functions using the separation of variable and exact boundary value technique. The unknown aperture field is expressed in terms of Fourier series with unknown expansion coefficients. The expansion coefficients are found by applying the boundary conditions on different surfaces and employing the addition theorem and orthogonality properties of the Mathieu functions. The effects of some coating materials on electromagnetic wave propagation are presented. One of these materials is chiral media which can generate both co- and cross-polarized waves simultaneously. For some applications, this is a big advantage of this material with respect to other kinds of materials. For TM and TE cases some numerical results of the antenna gain for co- and cross-polarized waves are presented and discussed. In general for the presented geometries, the slotted cylinders with chiral media-coating are offered more gain compared to other kinds of materials.

REFERENCES

1. Silver, S. and W. K. Saunders, "The external field produced by a slot in an infinite circular cylinder," *Jour. Appl. Phys.*, Vol. 21, 745–749, Aug. 1950.
2. Wait, J. R., *Electromagnetic Radiation from Cylindrical Structures*, Pergamon Press, Inc., New York, NY, 1959.
3. Wolff, E. W., *Antenna Analysis*, John Wiley & Sons, Inc., USA, 1966.
4. Hurd, R. A., "Radiation patterns of a dielectric coated axially-slotted cylinder," *Canadian J. Phys.*, Vol. 34, 638–642, 1956.
5. Mushref, M. A., "TM radiation from an eccentric dielectric coated cylinder with two axial slots," *Journal of Electromagnetic Waves and Applications*, Vol. 19, No. 5, 577–590, 2005.
6. Wong, J. Y., "Radiation conductance of axial and transverse slots in cylinders of elliptical cross section," *Proc. Inst. Radio Eng.*, Vol. 41, 1172–1177, 1953.
7. Wong, J. Y., "Radiation patterns of slotted-elliptic cylinder antennas," *IRE Transactions on Antennas and Propagation*, Vol. 3, 200–203, 1955.
8. Hussein, M., A. Sebak, and M. Hamid, "Scattering and coupling properties of a slotted elliptic cylinder," *IEEE Transactions on Electromagnetic Compatibility*, Vol. 36, No. 1, Feb. 1994.
9. Hinata, T. and H. Hosono, "Scattering of electromagnetic waves by an axially slotted conducting elliptic cylinder," *MMET'96 Proceedings*, 28–31, 1996.
10. Richmond, J. H., "Axial slot antenna on dielectric-coated elliptic cylinder," *IEEE Transactions on Antennas and Propagation*, Vol. 37, No. 10, Oct. 1989.
11. Ragheb, H. A., A. Sebak, and L. Shafai, "Radiation by axial slots on a dielectric-coated nonconfocal conducting elliptic cylinder," *IEE Proc. Microwave Antennas Propagation*, Vol. 143, No. 2, Apr. 1996.
12. Tsalamengas, J. L. and G. Veronis, "Radiation and receiving characteristics of parallel plate-fed slot antennas loaded by a dielectric cylinder: TE-case," *Journal of Electromagnetic Waves and Applications*, Vol. 13, 903–922, 1999.
13. Hamid, A. K., "Axially slotted antenna on a circular or elliptic cylinder coated with metamaterials," *Progress In Electromagnetics Research*, PIER 51, 329–341, 2005.
14. Khatir, B. N. and A. Sebak, "Coupling properties of slotted

- elliptic cylinder coated by dielectric/metamaterials,” *URSI GA08 Chicago, USA*, Aug. 7–16, 2008.
15. Erricolo, D., M. D. Lockard, C. M. Butler, and P. L. E. Uslenghi, “Numerical analysis of penetration, radiation, and scattering for a 2D slotted semielliptical channel filled with isorefractive material,” *Progress In Electromagnetics Research*, PIER 53, 69–89, 2005.
 16. Khatir, B. N. and A. Sebak, “Transverse electric wave scattering by parallel two-layer elliptic cylinders,” *EMTS, Ottawa, Canada*, Jul. 2007.
 17. Khatir, B. N. and A. R. Sebak, “Electromagnetic wave scattering by parallel dielectric/metamaterial coated elliptic cylinders,” *International Review on Modelling and Simulations (IREMOS)*, 41–48, Aug. 2008.
 18. Kluskens, M. S. and E. H. Newman, “Scattering by a chiral cylinder of arbitrary cross section,” *IEEE Transactions on Antennas and Propagation*, Vol. 38, No. 9, Sep. 1990.
 19. Kluskens, M. S. and E. H. Newman, “Scattering by multilayer chiral cylinder,” *IEEE Transactions on Antennas and Propagation*, Vol. 39, No. 1, Jan. 1991.
 20. Al-Kanhal, M. A. and E. Arvas, “Electromagnetic scattering from a chiral cylinder of arbitrary cross section,” *IEEE Transactions on Antennas and Propagation*, Vol. 44, No. 7, 1041–1048, Jul. 1996.
 21. Khatir, B. N. and A. Sebak, “Transverse electric wave scattering by elliptic chiral cylinder,” *ANTEM/URSI 2006, Canada*, Jul. 2006.
 22. Khatir, B. N., M. Al-Kanhal, and A. Sebak, “Electromagnetic wave scattering by elliptic chiral cylinder,” *Journal of Electromagnetic Waves and Applications*, Vol. 20, No. 10, 1377–1390, 2006.
 23. Sebak, A., H. A. Ragheb, and L. Shafai, “Plane wave scattering by a dielectric elliptic cylinder coated with nonconfocal dielectric,” *Radio Science*, Vol. 29, No. 6, 1393–1401, Nov.–Dec. 1994.
 24. Sebak, A. and L. Shafai, “Generalized solutions for electromagnetic scattering by elliptical structures,” *Computer Physics Communications*, Vol. 68, 1990.
 25. Ragheb, H. A., L. Shafai, and M. Hamid, “Plane wave scattering by a conducting elliptic cylinder coated by a nonconfocal dielectric,” *IEEE Transactions on Antennas and Propagation*, Vol. 39, No. 2, Feb. 1991.